SPE
Society of Petroleum Engineers

SPE 24040

Surveillance of South Belridge Diatomite

T.W. Patzek, Shell Western E&P Inc.
SPE Member

This paper was prepared for presentation at the Western Regional Meeting held in Bakersfield, California, March 30–April 1, 1992.

Abstract

This paper illustrates the surveillance methods used in Shell's 1-1/4 and 5/8 acre (0.5 and 0.25 ha) waterfloods in the South Belridge Diatomite field: (1) computer-assisted monitoring of injection pressures and rates, (2) online databases with well tests and allocated production and injection data, (3) step pressure tests in numerous water injectors, (4) a geological database with cycle markers and directional surveys, (5) sonologs, and (6) salinity tests. Methods (1) – (4) require use of custom software to be practical.

The geometry of waterflood patterns in the Diatomite (well spacing compared with length of hydrofractures, injectors in-line with or offset from producers, and pattern orientation relative to the direction of maximum in-situ stress) influences the rate and frequency of coupling between the injectors and producers. It is shown that wells in the "direct" 1-1/4 acre patterns are less prone to coupling than the "staggered" ones because a "linkage potential" (defined in the text) is higher.

The proximity of hydrofractures in the 5/8 acre staggered patterns makes the injector-producer coupling unavoidable if the patterns do not follow the direction of maximum in-situ stress. The coupling develops in the $N20^0 \pm 5^0 E$ direction, probably along the cycle tops.

The step pressure tests of many injectors in waterflood Phases I through III have shown that hydrofracture extensions are common and we are currently unable to predict the "correct" injection pressures for individual wells. It is concluded that to avoid reservoir damage, each injector must be controlled individually. Injection pressures can be increased with time by trial-and-error, but the injection rate must be kept below a safe limit to preclude excessive damage if the hydrofracture is extended.

Introduction

The South Belridge Field, Kern County, California, is located near the western margin of the San Joaquin Basin. Geologically [1], the field (Fig. 1) is a NW-SE trending anticline, approximately 7 miles (11 km) east of the San Andreas Fault. Oil production in the South Belridge Field comes from two major pay intervals, (a) the shallow marine Pleistocene Tulare sands, and (b) the marine Miocene–Pliocene Diatomite/Brown Shale. The latter interval has several unusual rock properties that make it unique. The rock has high porosity (50–70%) that is composed of several different pore types (interparticle, intraparticle, moldic, and fractures). The particle and pore sizes are small (0.1–100 μm). The matrix is chemically unstable and the grain density varies from 2 to 2.5 g/cm^3. Despite a high pore volume compressibility (100-300 μsips ($14.5\text{-}43.5 \times 10^{-6}$ kPa^{-1})), the rock contains natural fractures, some of which may be open, i.e., *not* cemented. The lithology of the Diatomite is the end-effect of cyclic variations in depositional environments that yielded a series of stacked silica-rich layers (cycles D – N in Fig. 1), separated by low permeability clay barriers. A typical cycle consists of a low quality clay/silt-rich interval overlaid by an increasingly pure diatomite deposition. This trend continues until a subsequent terrigenous influx marks the beginning of the next cycle. A functional definition of the top of the Brown Shale is the point (Fig. 1) below which the matrix porosity falls beneath 60% across most of the interval. Because the Diatomite/Brown Shale contact depends on diagenesis, it cuts across stratigraphic markers. Initially, the Diatomite was developed on a 2-1/2 acre (1 ha) spacing, with each well hydrofractured in several (3-6) stages over most of the interval. Since January 1987, the original patterns in Sections 33, 29, and 34 were gradually

†Currently with U. C. Berkeley.
References and illustrations at the end of paper.

infilled and converted to 1-1/4 acre (0.5 ha) staggered line waterfloods (Phase I, II, and III in Fig. 1) discussed in this paper.

Pattern Geometry

This section explains how the pattern layout may cause some hydrofractured wells to link faster than others. The 1-1/4 acre (0.5 ha) waterflood patterns in the Diatomite were laid N-S with the injectors either in line with or offset from the producers (Fig. 2). There are several "direct" patterns in Phase IA, but all other patterns in the Diatomite are offset or "staggered". The N-S pattern orientation does not follow the direction of least principle stress ($N15^0 \pm 15^0E$) [2], so in every pattern the hydrofracture planes of the NE and SW producers are closer to those of injectors. The injector-producer coupling may occur either between the fracture tips or two overlapping fractures (Fig. 2). Note that the cross-sectional area of flow and pressure gradient both favor coupling of the overlapping fractures. In the latter case, the coupling actually develops in the E-W direction, perhaps normal to the hydrofracture planes. This *real* direction must be distinguished from an *apparent* one, which is a function of well spacing and pattern orientation relative to the direction of maximum in-situ stress.

Fig. 3a plots the geometrical fracture-fracture distance vs. fracture half-length and azimuth. Because hydrofractures overlap in the staggered pattern, the distance between the fracture planes depends only on the azimuth. In the direct pattern, however, the tip-to-tip fracture distance decreases with fracture length until the fractures overlap. We may note that for hydrofracture design lengths between 110 and 135 ft (33–41 m), the direct pattern provides more separation between the fractures (and lesser driving force for flow). Therefore, one might expect the staggered pattern wells to link faster. Fig. 3b compares staggered patterns on 1-1/4 and 5/8 acre (0.5 and 0.25 ha) spacing by plotting a dimensionless linkage potential vs. fracture half-length for several fracture azimuths. The linkage potential is defined here as a ratio of fracture overlap to fracture-fracture distance. For uniform and constant pressures in the hydrofractures and constant fracture heights, this ratio is directly proportional to the cross-sectional area of flow multiplied by the pressure gradient, i.e., to the flow rate. All other factors being equal, the 5/8 acre (0.25 ha) pattern has a 3-4 times higher linkage potential than its 1-1/4 acre (0.5 ha) counterpart. In other words, if the injector-producer coupling were to occur within 200 days in 1-1/4 acre patterns, one would expect it to occur within 70 days on 5/8 acre spacing.

There are two complementary mechanisms of injector-producer coupling. The probability of the first one, through natural fractures, is proportional to the density of *open* natural fractures in the rock and depends on the orientation of these fractures relative to the hydrofracture plane. Fig. 4 shows the number frequency of natural fractures versus their azimuths in oriented cores from three Diatomite wells. If the hydrofracture azimuth is assumed to be 65^0, then the direction perpendicular to the fracture is 155^0 (mirror reflection confines the azimuths to $0–180^0$). Fig. 4 shows that a majority of natural fractures intersect the hydrofracture at 45^0 or more, and can be conduits for flow if open. Recently, a vertical hydrofracture in cycles K through M (cf. Fig. 1) was successfully imaged [3, 4] and hundreds of microseismic events were recorded at different stages of growth of the fracture. Many of these events occurred along the tops of two cycles (K and M), away from the hydrofracture plane [4] (along the 155^0 azimuth in Fig. 4 because of mirror reflection). It also appears [3, 4] that on each side of the hydrofracture plane there exist 30-50 ft (9–15m) wide disturbed zones which are confined to the upper portions of the cycles. Natural fractures did play a role in the creation of these disturbed zones, but there might be another mechanism. The top or high porosity part of each depositional cycle is cleaner, i.e., it contains more amorphous silica (diatoms) which with time and increased temperature undergo a diagenetic transformation to Opal CT and release inter-crystalline water. Because rock layers with a higher fraction of diagenetic material are surrounded by impermeable seals, the released water cannot easily escape. This leads to overpressuring of the altered rock, reduction of the effective stress, and increased probability of inducing hydrofractures [5] at the cycle boundaries.

By assuming average lengths and azimuths of hydrofractures, one can calculate the distribution of fracture-fracture distances. The necessary surface locations and directional surveys of the Diatomite wells have been acquired from a geological database. Figs. 5 and 6 are but two examples of such distributions, plotted for the Phase IA and IB wells as deviations from the ideal geometric distances between the fractures. Compared to ideal direct patterns, the tips of producer hydrofractures in Phase IA are up to 50 ft (15 m) closer to those of the adjacent NE and SW injectors (Fig. 5) for 70% of the wells. The deviations greater than 50 ft (15 m) reflect the presence of open hydrofractures in the plugged-and-abandoned wells that failed and were replaced. The Phase IB staggered producers (Fig. 6) are broadly scattered about their geometric locations, with 40% of the wells being 50 ft (15 m) closer than ideal to the adjacent NE and SW injectors. In conclusion, Phase IB wells might link faster than those in Phase IA only because the linkage potential is higher in the staggered patterns.

The close spacing of hydrofractures in the 5/8 acre (0.25 ha) staggered patterns (Fig. 7) makes the injector-producer linkage unavoidable, as observed in the seven-pattern, 5/8-acre waterflood pilot in Section 33. In addition, the high pore pressure (low effective stress) regions around the converted 1-1/4 acre injectors may attract [6] the new hydrofractures in the infill wells, further exacerbating the coupling problem.

It is important to remember that an *apparent* direction of the injector-producer coupling ($N18.4^0E$) is defined by the N-S layout of the 5/8 acre patterns (Fig. 7) and, to some degree, it is insensitive to the direction of maximum in-situ stress. Similarly, in the 1-1/4 acre direct and staggered patterns the *apparent* linkage directions are $N26.5^0E$ and $N45^0E$, respectively (Fig. 2). The usually NW deviations

from these directions are caused by those producers that are closer than ideal to the injectors and are more likely to link (cf. Figs. 5 and 6).

Phase I Waterflood

This section briefly describes the history of water injection in the Phase I waterflood in Section 33 (cf. Fig. 1). A six-injector, limited interval waterflood pilot was started in September 1982, to test water injectivity in cycles J through M in the best part of Section 33. In February 1985, a single-injector (575N-33), full-interval pilot was initiated. Almost two years of water injection at 5000 BWPD (795 m^3/d) extensively fractured the reservoir around the pilot. Full-scale water injection in Phases IA (direct pattern) and IB (staggered pattern) dual-string wells was started in January 1987 and August 1988, respectively. As one can see, the Phase I waterflood in Section 33 has been a proving ground for several water injection schemes and injector designs. This makes the interpretation of Phase I quite difficult, but enables one to look at various stages of waterflood projects and reservoir damage.

From a total of 128 producers and 94 injectors drilled in the Phase I area, there have been 34 high-gross producers and 49 high-rate injectors (Fig. 8). The areal distribution of these high-rate wells is shown in Fig. 9; it is intuitively obvious that both injector-producer coupling and reservoir damage have occurred. In particular, there is a three-pattern-wide SW-NE corridor of damaged reservoir across the western part of Section 33 and a cluster of high-rate wells around injector 575N-33 in the SE part.

Figs. 10-12 compare the allocated injection and production rates of "High Rate" (continuous curve) and "Other" (broken curve) wells versus time elapsed from the initiation of water injection in Phase IB. The initial "High Rate" injection ramp in Fig. 10 (between -1000 and -500 days) was caused by the single-injector pilot; the "Other" injection was in the six-injector pilot. The peaks between -300 and 0 days correspond to the start of injection in Phase IA, followed by conversions and injection in Phase IB. Fig. 10 shows that 50% of the Phase I injectors took only 10-20% of the water. Fig. 11 plots oil production rates for both well sets. The peaks correspond to 1-1/4 acre (0.5 ha) infills in Phases IA and IB. These rates then decline as the square-root of time on production. Fig. 12 paints a dramatically different picture of water production; as the "Other" category water rate declines, the "High Rate" water production continues to climb. Note that the "High Rate" wells produce twice as much water as the "Other" category.

The delay time for injector-producer linkage was about 180 days (cf. Fig. 12). It is also quite obvious that water broke through in limited intervals and oil production from the high-gross wells has not been impaired significantly. Interestingly, water produced by the high rate wells has amounted to only 20% of "High Rate" injection (Fig. 13). In other words, 80% of the injected water might not have gone into the matrix but created flow paths outside the waterflood area. Usually, a severe imbalance of injection and production is a symptom of hydrofracture extension beyond the project area and, indeed, fluid kicks were observed during drilling operations in the West Flank Shallow area, more than 700 ft (213 m) from the waterflood boundary.

There are numerous examples of injector-producer coupling in the Phase I waterflood. Such a coupling has caused at least 35 Phase I producers to free flow. Most of these wells have been killed or permanently abandoned. Figs. 14–16 show three such examples with various degrees of coupling. Fig. 14 plots water production rates from 552-33 (solid curve) versus days on injection in 552NR-33, long string (LS-broken curve) and short string (SS-dotted curve). The injector is 140 ft (43 m) SE from the producer and the fracture overlap is 230 ft (70 m). Well 552-33 began free-flowing just after injection was started in 552NR-LS at 1500 BWPD (238 m^3/d). No well tests were performed for 1-1/2 years, but when the tests were resumed, water production in 552-33 followed almost exactly the injection in both strings of 552NR-33. Therefore, well 552-33 linked to at least one of the injection strings and produced the injected water. Fig. 15 shows a not-so-strong coupling between producer 543A-33 and dual-string injector 544E-33. In this example, the producer responds almost instantaneously to the injector and produces approximately 1/3 of water injected into the short string (note that initial production exceeds the long string injection). It is remarkable how quickly the linkage occurred over a 120 ft (37 m) distance. Fig. 16 is an example of a rare tip-to-tip coupling between producer 543S-33 and injector 544G-33. The producer links to the long string of the injector and becomes constrained by the pump lift capacity. Note that this tip-to-tip coupling took more than 300 days across a 110 ft (34 m) distance.

In conclusion, injector-producer coupling is a real problem in the Diatomite. If it occurs, most of the injected water is recirculated through the hydrofractures and does not enter the matrix. This diminishes the waterflood effectiveness and increases lift costs. When the producing wells cannot be pumped off due to a limited lift capacity, oil production also decreases. In addition, the reservoir pressuring by water injection becomes non-uniform and the areally uneven formation uplift or subsidence results in increased well failures. (It is not a coincidence that the high-injection corridor in Section 33 (Fig. 9) is directly east from an area with the highest rate of well failures. As the total injection into this corridor is lowered, the rate of well failures should also go down.)

Seven Pattern, 5/8 Acre Waterflood Pilot

The seven-pattern, 5/8 acre (0.25 ha) waterflood pilot in Phase II spans the NW part of Section 33 and SW part of Section 28 (Fig. 17). The goal of this pilot was to check the preferred direction and rate of injector-producer coupling in the 5/8 acre staggered patterns. To achieve this goal, only half of the wells in the injector locations were converted to injectors. The remaining half were left on production and monitored for water breakthrough.

On September 25, 1989, step pressure tests were initiated in all 11 pilot injectors. Injection was started with a pres-

sure gradient of 0.48 psi/ft (10.9 kPa/m) to the top of the M cycle and a rate limit of 450 BWPD (72 m^3/d). Individual injection pressure gradients were then increased in 0.02 psi/ft (0.45 kPa/m) increments, as appropriate, and the injectors have linked to the adjacent SW and NE producers in the N20°±5°E direction at injection gradients below 0.6 psi/ft (13.6 kPa/m).

There are several indications of injector-producer linkage: (1) producers that are not pumped-off, (2) produced brine salinities that are significantly lower than the in-situ salinity, and (3) increases in injection that coincide with increased gross rates from offset producers. The coupling of producer 531E1-33 with injector 531L-33 and then 538A-33 is a good example of all three phenomena. Fig. 18 shows the results of sonologs in the pilot producers suspected of linking with the adjacent injectors. The logs show high fluid levels (i.e. wells that are not pumped-off). In particular, producer 531E1-33 shows one thousand feet of fluid above the pump. Fig. 19 plots the results of water and oil tests in 531E1-33 versus days of water injection in the pilot. Note that the water rate has increased to 700 BWPD (111 m^3/d) somewhere between 30 and 140 days of injection. Water breakthrough in 531E1-33 can be defined better by looking at the injection rates in 531L-33 and 538A-28 (Figs. 20–21). Injector 531L-33 injected water at the rate limit for the first 70 days (conceivably, it could link to 531E1-33 almost instantaneously). Thereafter, the rate decreased and the wellhead pressure increased from vacuum to 70 psig (584 kPa) (set-point for the first pressure step). In contrast, injector 538A-28 went on vacuum after 63 days of injection, and its rate jumped up to the limit. After 70 days, the combined injection in the two wells was 750 BWPD (119 m^3/d), roughly equal to the water production rate from 531E1-33. A produced brine salinity test in 531E1-33 showed a significant shift from the in-situ salinity of 30,000 ppm Cl to the injected salinity of roughly 9,000 ppm Cl (Fig. 22). To summarize, producer 531E1-33 linked to both adjacent injectors within the first 70 days of injection, about 1/3 of the average linkage time on 1-1/4 acre spacing. Several other pilot producers (531C1-33, 533E-33, 533C-33 and 533C1-33) linked within the same time period.

All injector-producer coupling has occurred along the apparent azimuth of N20°E (Fig. 7). In addition, because of relatively low injection rates, water broke through only in limited intervals and primary oil production from other intervals has not been impaired. On the other hand, water injection into the matrix *has* been impaired. Conversion of linked producers to injectors, either active (injecting water) or passive (no injection string or flowline), could help.

The 5/8 acre (0.25 ha) N-S staggered patterns are prone to coupling. This finding has important practical implications: (a) Injector-producer linkage in the 1-1/4 acre patterns may preclude future 5/8 acre development (Fig. 23) and (b) Implementation of a 5/8 acre development will require conversion of half of the 1-1/4 acre injectors back to producers.

Step Pressure Tests

The results of step pressure tests in some 50 wells in Phases I, II and III show that we are currently unable to predict the "correct" injection pressures for individual wells. Figs. 24–26 depict the extreme sensitivity of injection rate to changes in injection pressure and illustrate the importance of the Computer-Assisted Operations (CAO) system for Diatomite waterfloods. The CAO system made it possible to acquire 1-hour averages of 1-minute readings of injection rates and wellhead pressures for many injectors over long periods of time. The active (injecting) hydrofracture areas, calculated for each pressure step (Appendix A), are plotted relative to that during the first step. In turn the injection areas during the first pressure step are listed in each figure for two limiting cases of (a) free gas going into solution and (b) oil above the bubble point. The first limiting case is likely to apply more to the new Phase IIIA and 5/8-acre waterflood pilot injectors, whereas the second one to those in the mature Phase I. As injector 555E-33 was restarted in a pressured-up area of Phase I, the water-hammer caused by a jump in pressure from 0 to 200 psi (0–1379 kPa) extended the hydrofracture and incremental 20 MB (3180 m^3) of water were injected during the next 60 days (Fig. 24). Similar behavior was observed in a depleted area in Phase IIIA. A 0.02 psi/ft (0.45 kPa/m) increase in pressure gradient resulted in a 600 BPD (95 m^3/d) jump in well 537E-34, and incremental 20 MBW (3180 m^3) were injected during the next 60 days (Fig. 25). The sudden drop of injection rate after 170 days was caused by setting the maximum injection rate to 450 BWPD (72 m^3/d). Note that the calculated fracture extension in well 537E-34 is twice as severe as that in injector 555E-33. A new injector 531A1-33 in the seven pattern, 5/8-acre waterflood pilot experienced fracture extensions during each pressure step (Fig. 26). Further fracture extensions were limited by setting the maximum allowed injection rate to 450 BWPD (72 m^3/d). Depending whether oil was below or above the bubble point, the calculated active fracture areas were up to 0.3–2, 0.5–4.5, and 0.3–2.5 times the design areas for 555E-33, 537E-34, and 531A1-33, respectively. If history of an injection well (time on production, gross rate, BHP) prior to conversion is neglected or unknown, then the *absolute* values of fracture areas may be inaccurate. The *relative* changes of these areas, however, should be modeled fairly well. In conclusion, to avoid reservoir damage, each injector must be controlled individually. Injection pressures can be increased with time by trial-and-error, but the injection rate must be kept below a safe limit to preclude excessive damage if the hydrofracture is extended.

Conclusions

1. Well pattern and fracture geometry define order of injector-producer coupling.
2. Coupling between the injectors and producers on 1-1/4 acre spacing can be avoided or minimized.
3. In the 5/8 acre N-S staggered patterns, injectors link with adjacent SW and NE producers in the apparent

N20^0±5^{0}E direction.

4. If the injector-producer coupling develops E-W on 1-1/4 acre spacing, the subsequent 5/8 acre development may become unfeasible.

5. The unique properties of the Diatomite rock make it very difficult to specify correct injection rates for every well.

6. To prevent excessive growth of hydrofractures, a conservative water injection policy should be implemented and injectors be controlled individually with help of an appropriate Computer-Assisted Operations system.

7. Such a policy will result in more uniform injection into the matrix and reduce the potential of well failures due to localized strain.

Acknowledgements

I would like to thank Shell Western E&P, Inc., for permission to publish this paper. Drs. P. D. Patel and S. K. Hara reviewed the manuscript and provided valuable advice. Mr. R. E. Oligney was instrumental in planning and execution of the step pressure tests.

NOMENCLATURE

A = fracture area, ft^2 [m^2]
^{0}API = API oil gravity
B = FVF, rb/stb [res m^3/stock-tank m^3]
c = compressibility, psi^{-1} [kPa^{-1}]
D_j = mid-depth of jth fracture interval, ft [m]
k = permeability, md
K = compaction coefficient, psi^{-1} [kPa^{-1}]
p = pressure, psia, [kPa]
q = rate, bpd [m^3/d]
R_s = solution GOR, scf/stb [std m^3/stock-tank m^3]
S = saturation
t = time, d [s]
T = temperature, °F [°C]
α = hydraulic diffusivity, ft^2/d [m^2/s]
γ = specific gravity
μ = viscosity, cp [mPa·s]
ϕ = porosity

Subscripts

f = fracture
g = gas
i = ith pressure step
j = jth fracture interval
o = oil
r = rock
s = solution
T = total
w = water
wh = well head
0 = initial conditions
ϕ = pore volume

REFERENCES

1. Schwartz, D. E., Characterizing the Lithology, Petrophysical Properties, and Depositional Setting of the Belridge Diatomite, South Belridge Field, Kern County, California, in *Studies of the Geology of the San Joquin Basin*, Edited by S.A. Graham, SEPM Book #60, 281-301 (1988).
2. Hansen K. S. and Purcell, W. R., Earth Stress Measurements in the South Belridge Oil Field, Kern County, California, Paper SPE 15641, presented at the 61st Annual Technical Conference and Exhibition of the SPE, New Orleans, LA, Oct. 5-8 (1986).
3. Vinegar, H. J., Wills, P. B., De Martini, D. C., Shlyapobersky, J., Deeg, W. F. J., Adair, R. G., Woerpel J. C., Fix, J. E. and Sorrells, G. G., Active and Passive Seismic Imaging of a Hydraulic Fracture in Diatomite, Paper SPE 22756, presented at the 66th Annual Technical Conference and Exhibition of the SPE, Dallas, TX, Oct. 6-9 (1991).
4. Patzek, T. W., Gritto, R., Ilderton D., Majer, E. L., Microseismic Imaging of a Hydrofracture in Diatomite, to be submitted to *J. Geophys. Res.* (1992).
5. Bruno, M. S. and Nakagawa, F. M., Pore Pressure Influence on Tensile Fracture Propagation in Sedimentary Rock, *Int. J. Rock Mech. Min. Sci. & Geomech. Abstr.*, Vol. 28, No.4 261-273 (1991).
6. Finol, A. and Farouq Ali, S. M., Numerical Simulation of Oil Production With Simultaneous Ground Subsidence, *Trans.* AIME, 411-424 (1975).
7. Chase, C. A., Jr. and Dietrich, J. K., Compaction Within the South Belridge Diatomite, *SPERE*, 422-428, Nov. 1989.
8. Meehan, D. N., A Correlation for Water Compressibility, *Pet. Engr.*, 125-126, Nov. 1980.
9. Standing, M. B., Volumetric and Phase Behavior of Oil Field Hydrocarbon Systems, 9th Ed. Dallas: SPE (1981).

APPENDIX A

Muliple-step pressure tests were used in the Diatomite waterflood projects to determine the fracture propagation pressure and/or injectivity impairment. In all tested wells, the downhole injection pressures were controlled as

$$p_i = \left(\frac{\partial p}{\partial D}\right)_i \times D_{\text{Top of M Cycle}}, \quad i = 1, 2, ..., N, \quad \text{(A-1)}$$

with $(\frac{\partial p}{\partial D})_i$ initially set to 0.48 psi/ft (10.9 kPa/m) and then increased in 0.02 psi/ft (0.45 kPa/m) increments at each step i. The wellhead injection pressure was then back calculated from Eq. (A-1) as

$$p_{\text{wh}_i} = p_i - 0.44 * D_{\text{Top of M Cycle}} \quad \text{(psia)}. \quad \text{(A-2)}$$

Therefore, history of the downhole injection pressure in

each well can be described as

$$p(x=0,t) = p_0 + \sum_{i=1}^{N} (p_i - p_{i-1})\, \mathbf{1}(t - t_{i-1}), \qquad \text{(A-3)}$$

where $\mathbf{1}(t - t_i)$ is the Heaviside unit function equal to 1 if $t - t_i \geq 0$ and 0 otherwise. If we assume that the hydro-fracture has infinite conductivity, we can interpret the results of the tests from a solution of the pressure diffusion equation in linear flow

$$\frac{\partial^2 p}{\partial x^2} = \frac{1}{\alpha}\frac{\partial p}{\partial t}, \qquad \alpha \equiv \frac{k_w}{\phi \mu c_T}. \qquad \text{(A-4)}$$

Subject to the initial condition

$$p(x,0) = p_0, \quad \text{everywhere}, \qquad \text{(A-5)}$$

boundary condition (A-3), and

$$\lim_{x \to \infty} p(x,t) = p_0 \quad \text{for all } t > 0, \qquad \text{(A-6)}$$

Eq. (A-4) has a linear superposition solution

$$p(x,t) = \sum_{i=1}^{N} (p_i - p_{i-1}) \operatorname{erfc}\left[\frac{x}{2\sqrt{\alpha(t - t_{i-1})}}\right], \quad t > t_{N-1}, \qquad \text{(A-7)}$$

where erfc is the complementary error function. The injection rate of water is

$$\begin{aligned} q(t) &= -2A_f \frac{k_w}{\mu}\left(\frac{\partial p}{\partial x}\right)_{x=0} \\ &= \frac{2}{\sqrt{\pi}} A_f \sqrt{\frac{k_w \phi c_T}{\mu}} \sum_{i=1}^{N} \frac{p_i - p_{i-1}}{\sqrt{t - t_{i-1}}}, \\ &\quad t > t_{N-1}. \end{aligned} \qquad \text{(A-8)}$$

The Diatomite waterflood injectors have multiple hydro-fractures which may be considered as injecting into non-communicating layers. Thus

$$q(t) = \frac{2}{\sqrt{\pi}} \sum_{j=1}^{\#\text{ fracs}} A_{fj} \sqrt{\left(\frac{k_w \phi c_T}{\mu}\right)_j} \sum_{i=1}^{N} \frac{p_{ij} - p_{i-1,j}}{\sqrt{t - t_{i-1}}}, \quad t > t_{N-1}, \qquad \text{(A-9)}$$

where the initial reservoir pressure is approximated by

$$p_{0j} = 29.7 + 0.38 D_j \quad \text{(psia)}, \qquad \text{(A-10)}$$

$$p_{ij} = \text{const}, \qquad \text{(A-11a)}$$

for a pumped-off producer, and

$$p_{ij} = p_{\text{wh}_i} + 0.44 D_j \quad \text{(psia)}, \qquad \text{(A-11b)}$$

after conversion to a water injector. Note that time $t = 0$ corresponds to drilling a well in a virgin reservoir.

Calculation of c_T

In general, the total compressibility of the system is

$$c_T = c_\phi + S_w c_w + S_o c_o + S_g c_g. \qquad \text{(A-12)}$$

Depending on the injection conditions, oil is either below or above the bubble point and Eq. (A-12) has two limits, respectively. In the first limit

$$c_o = -\frac{1}{B_o}\left(\frac{\partial B_o}{\partial p} - B_g \frac{\partial R_s}{\partial p}\right), \qquad \text{(A-13)}$$

and in the second one $\partial R_s/\partial p$ is equal to zero.

Calculation of c_ϕ

The effective pore volume compressibility is [6, 7]

$$c_\phi = \frac{K + (1-\phi)c_r}{\phi} \approx 300\ \mu\text{sips}, \qquad \text{(A-14)}$$

because of high compressibility and compactibility of the diatomite.

Calculation of c_w

We assume that solubility of gas in water is negligible in both cases. Then the compressibility of gas-free water may be calculated from a correlation by Meehan [8]

$$\begin{aligned} c_w = 10^{-6}\big[&3.8546 - 0.000134p \\ &+ (4.77 \times 10^{-7} p - 0.01052)\, T \\ &+ (3.9267 \times 10^{-5} - 8.8 \times 10^{-10} p)\, T^2\big]\ (\text{psi}^{-1}). \end{aligned} \qquad \text{(A-15)}$$

Calculation of c_o

Standing [9] has developed correlations for B_o and R_s of 22 mixtures of California crudes. With few changes, these correlations can be used for the Diatomite oil

$$R_s = \gamma_g^* \left[\left(\frac{p}{6.4}\right) 10^{0.0125^0 API - 0.00091T}\right]^{0.968}, \qquad \text{(A-16)}$$

and

$$B_o = 0.9714 + 0.00035\left[R_s \sqrt{\frac{\gamma_g^*}{\gamma_o}} + 1.25\,T\right]^{1.021}, \qquad \text{(A-17)}$$

where

$$\gamma_g^* = 0.21\sqrt{\gamma_g\, {}^0API} - 0.36 \log p + 0.98, \qquad \text{(A-18)}$$

is a modified specific gravity of the solution gas.

Calculation of c_g

We assume that the free gas in the reservior is approximately ideal:

$$B_g \approx 0.005035\left(\frac{T + 460}{p}\right) \quad \text{rb/scf}. \qquad \text{(A-19)}$$

$$c_g \approx \frac{1}{p} \qquad \text{(A-20)}$$

All parameters in Eq. (A-9) are listed in Table A-1 and the fractured intervals in injection wells discussed in this paper in Table A-2, respectively.

Table A-1: Model Parameters

Parameter	Value	Units
Porosity ϕ	0.6	–
PV compressibility c_ϕ	300	μsips
Permeability k_w	0.05	md
Viscosity μ_w	1.0	cp
API oil gravity	29	^{0}API
Gas gravity γ_g	0.87	–
Water saturation S_w	0.65	–
Oil saturation S_o	0.34–0.35	–
Gas saturation S_g	0–0.01	–

Table A-2: Fractured Intervals (ft)

555E-33	537E-34	531A1-33
670–870	775–975	605–850
920–1140	1025–1225	900–1080
1190–1340	1275–1475	1130–1450
1390–1540	1525–1725	1500–1720*
1590–1720	–	–
1770–1820	–	–

* (Fracture radius = 1/2 Interval)

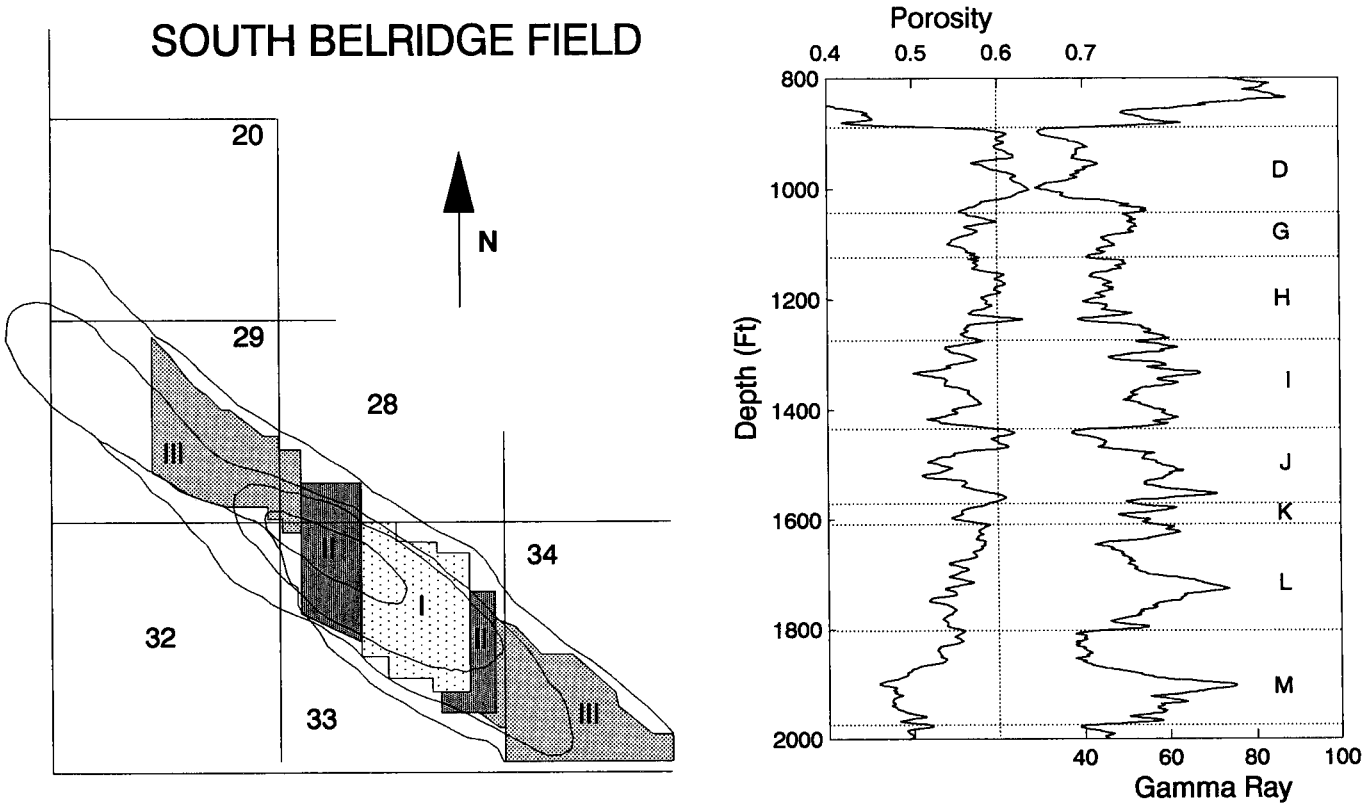

Fig. 1—Plan view and a typical cross section of the South Belridge field.

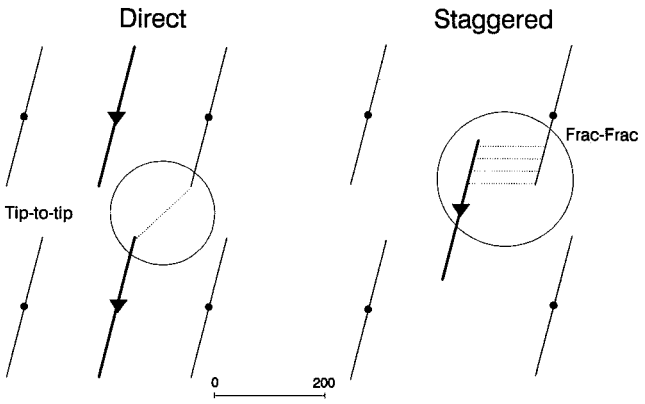

Fig. 2—How hydro-fractures may link in 1¼-acre (0.5-ha) direct and staggered line waterflood patterns. The assumed half-length and azimuth of the fractures is 135 ft (41 m) and N15°E, respectively.

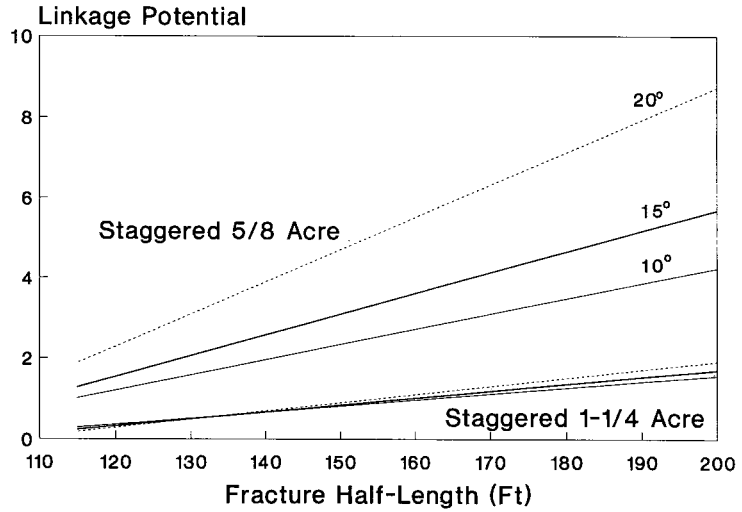

Fig. 3b—Dimensionless linkage potential for ⅝- and 1¼-acre (0.25- and 0.5-ha) staggered line patterns.

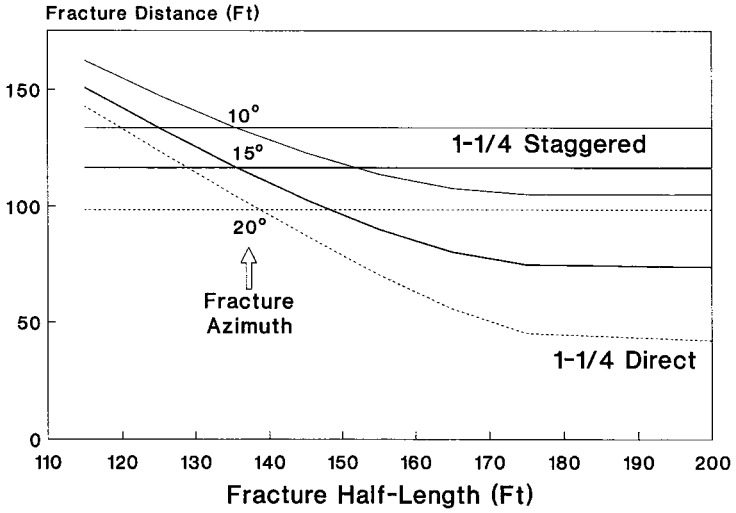

Fig. 3a—Fracture-fracture distance vs. fracture half-length for 1¼-acre (0.5-ha) direct and staggered line patterns.

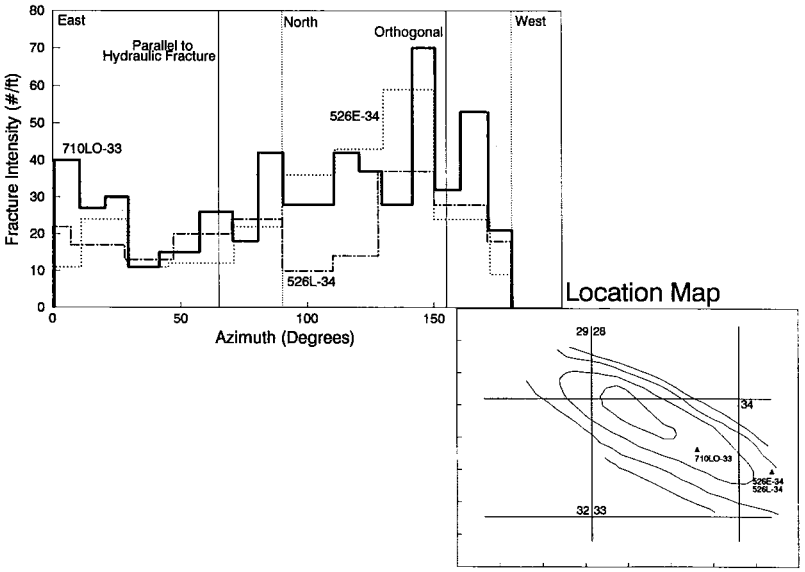

Fig. 4—Intensity of natural fractures vs. their azimuths (from oriented cores in the Diatomite Wells 526E-34, 526L-34, and 710LO-33).

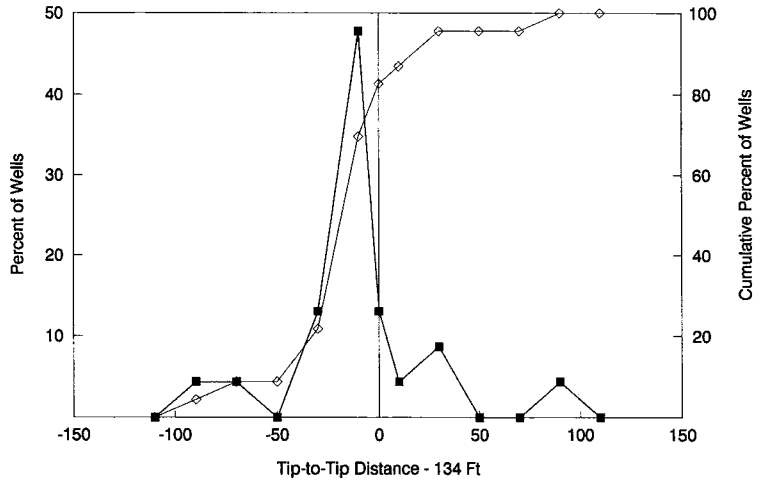

Fig. 5—The distribution of tip-to-tip distances between a producer hydro-fracture and that of an injector NE or SW from the producer for all the Phase IA producers (assumed fracture half-lengths and azimuths are 125 ft (38 m) and N15°E, respectively).

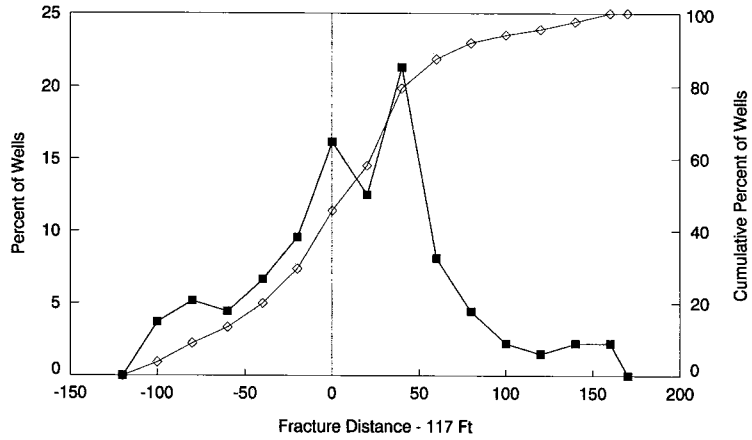

Fig. 6—The distribution of plane-to-plane distances between a producer hydro-fracture and that of an injector NE and SW from the producer for all the Phase IB producers (assumed fracture half-lengths and azimuths are 125 ft (38 m) and N15°E, respectively).

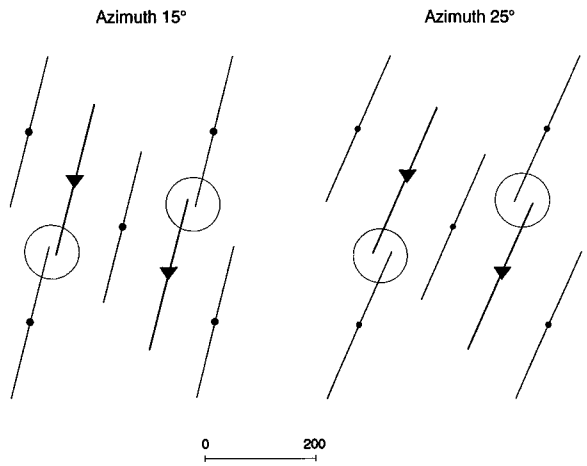

Fig. 7—Injector-producer linkage in the 5-acre (0.5-ha) staggered line waterflood pattern; the assumed half-length of hydro-fractures is 135 ft (41 m).

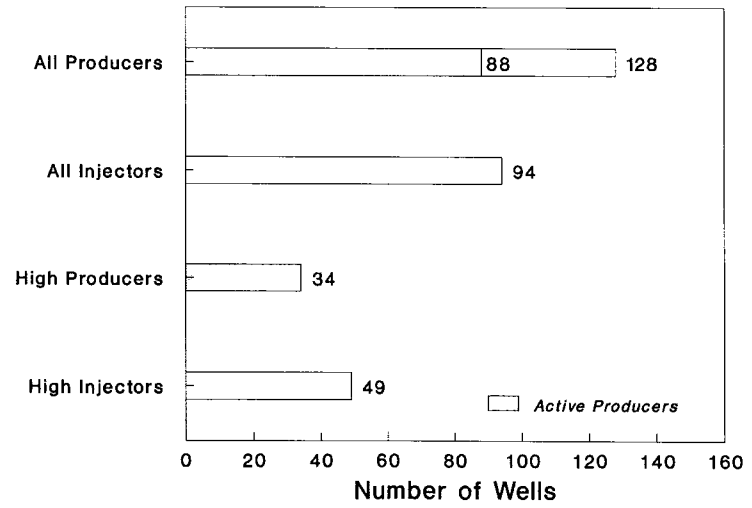

Fig. 8—Classification of wells in the Phase I waterflood (Section 33).

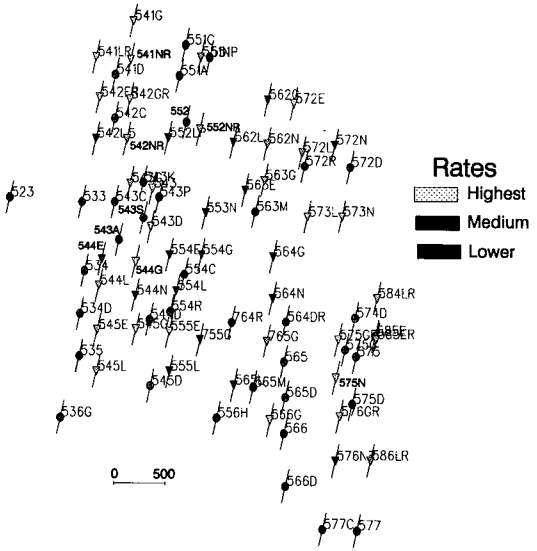

Fig. 9—Locations of "High Rate" wells in Phase I waterflood.

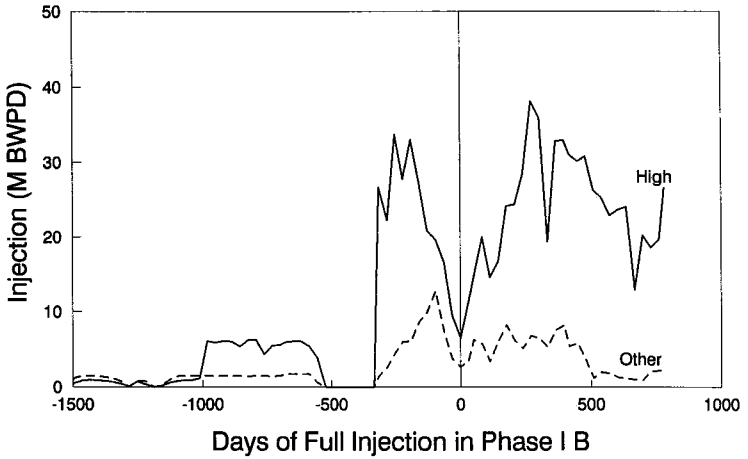

Fig. 10—Injection rate of water for the "High Rate" and "Other" Phase I waterflood injectors.

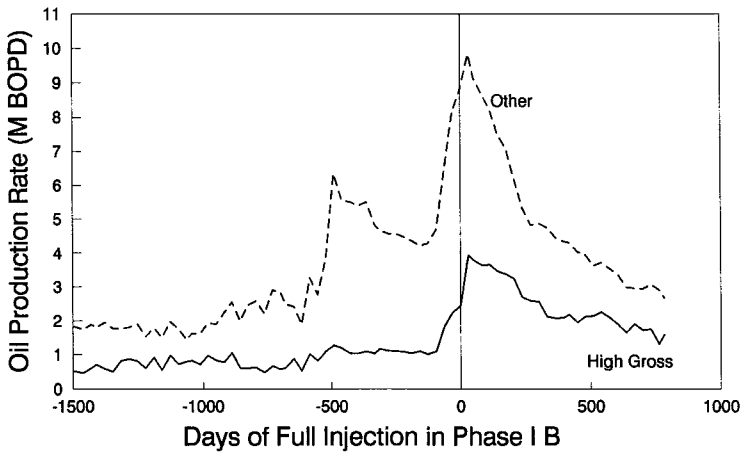

Fig. 11—Oil production rates for "High Gross" and "Other" wells in the Phase I waterflood. Note a steeper rate of decline in the "Other" category.

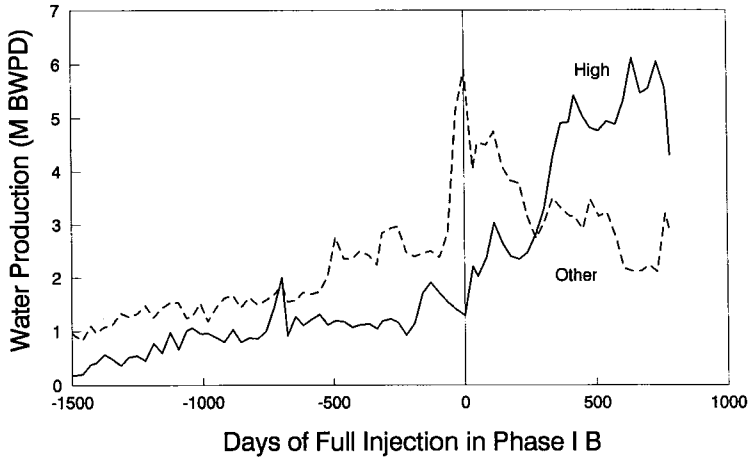

Fig. 12—Water production rates for "High Gross" and "Other" wells in the Phase I waterflood. Note that water production in the "High Gross" category kept on increasing until the injection rates were curtailed. In contrast the "Other" category rate declined as the square root of time. Note a dramatic increase of water production after 180 days of injection.

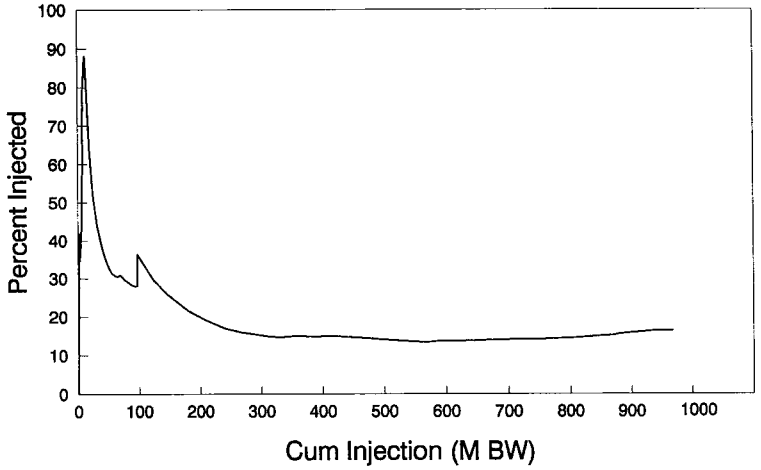

Fig. 13—Water produced by the Phase I "High Gross" wells as percent of cumulative injection in the "High Rate" injectors. Note the severe imbalance, suggestive of fracture extension and reservoir damage.

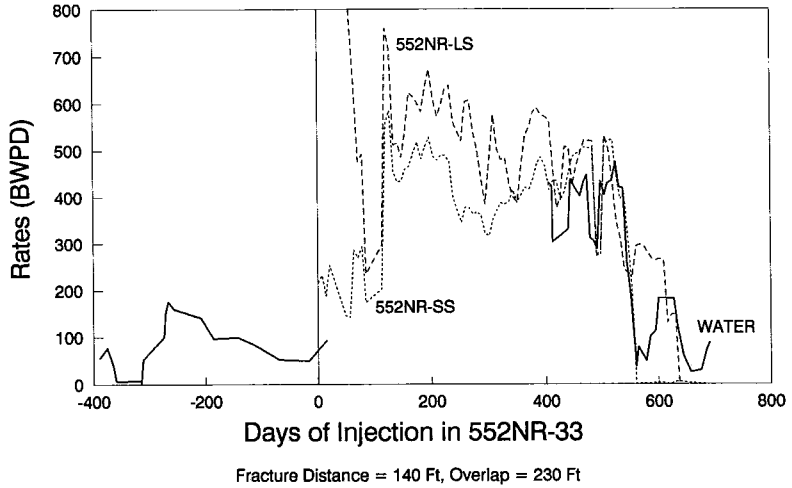

Fig. 14—Phase IB producer 522NR-33 links with the long injection string of the dual injector 552-33 and free flows.

Fracture Distance = 140 Ft, Overlap = 230 Ft

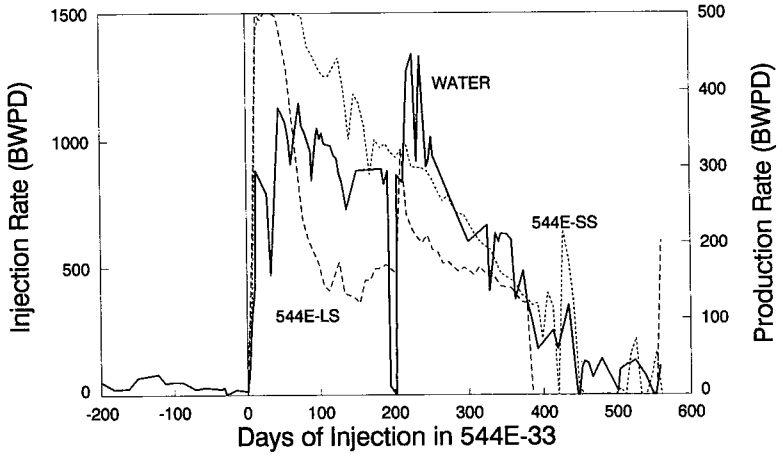

Fracture Distance = 120 Ft, Overlap = 60 Ft

Fig. 15—Phase IB producer 543A-33 links with the short injection string of the dual injector 544-33.

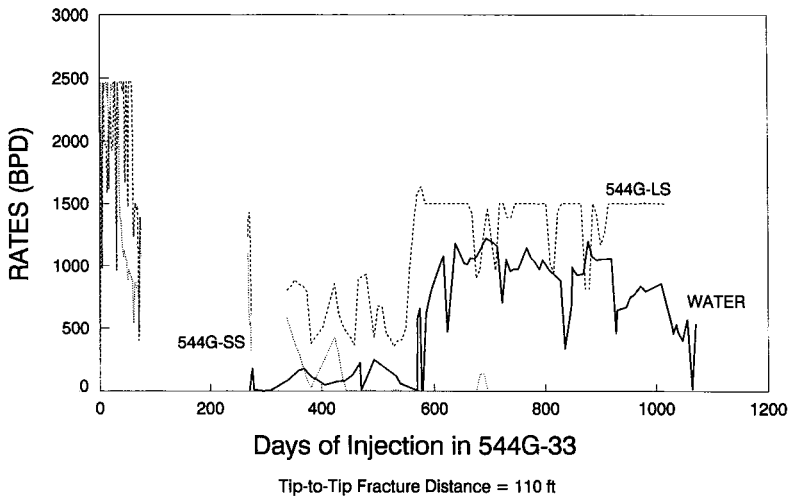

Fig. 16—Phase IB producer 543S-33 links with the long injection string of the dual injector 544G-33. The production rate is limited by the pump-lift capacity.

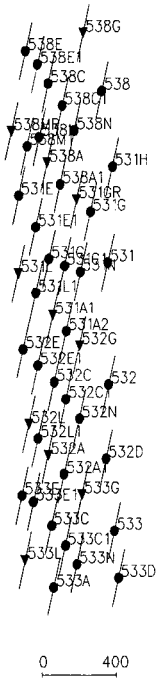

Fig. 17—Plan view of the seven-pattern, 5/8-acre waterflood pilot.

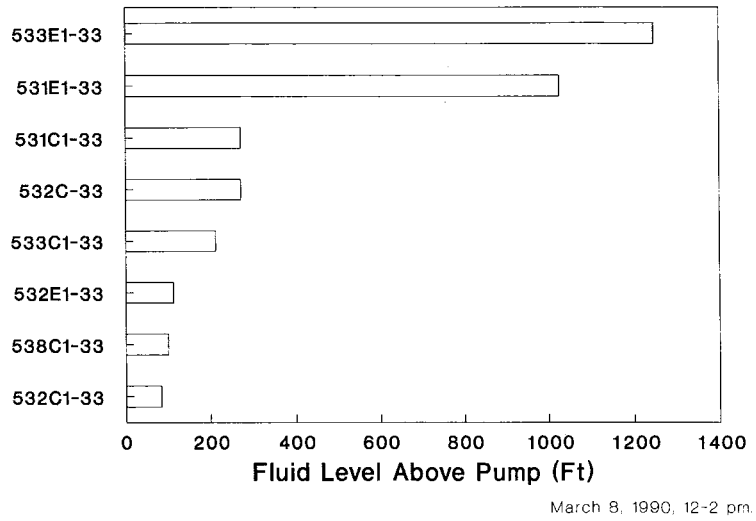

Fig. 18—Fluid levels in the high-gross producers in the seven-pattern, 5/8-acre waterflood pilot.

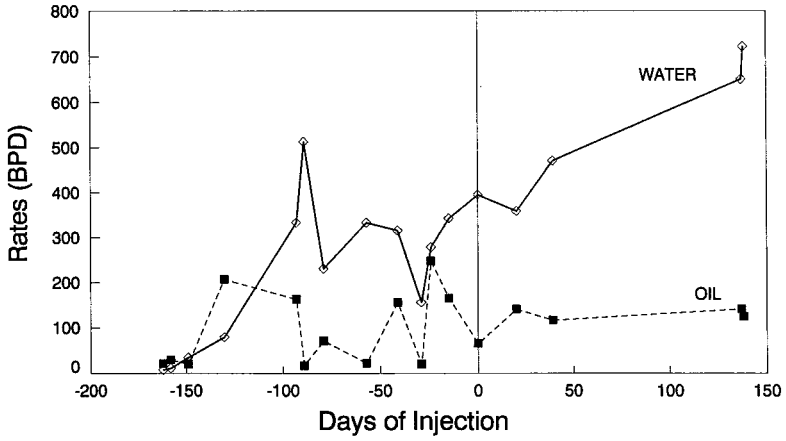

Fig. 19—Oil and water production rates in Well 531E1-33 that first linked with injector 531L-33 and then 538A-28. Note that no production tests were performed between 40 and 140 days.

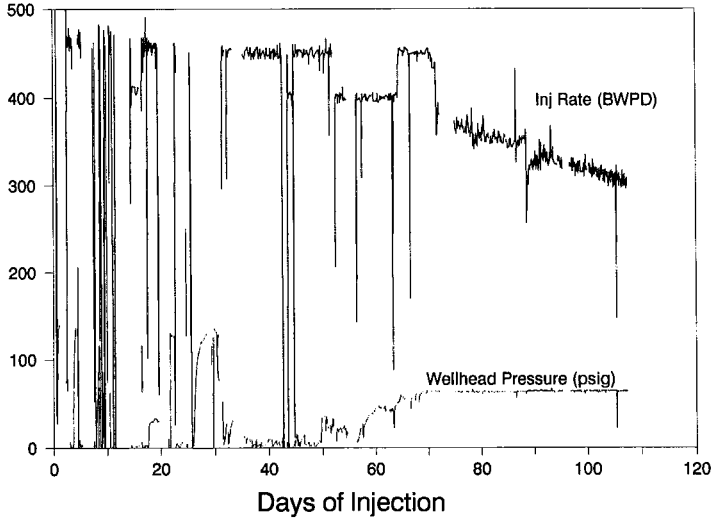

Fig. 20—Injector 531L-33 links with 531E1-33 and pressures up after 70 days of injection.

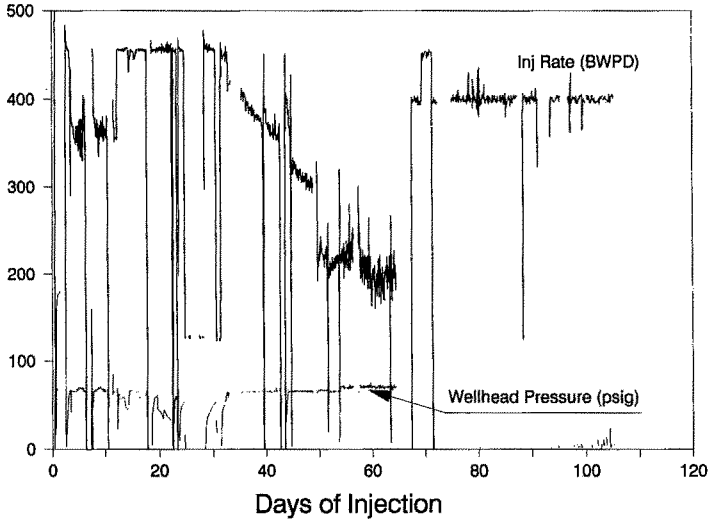

Fig. 21—Injector 538A-28 links with 531E1-33 after 62 days of injection and goes on vacuum.

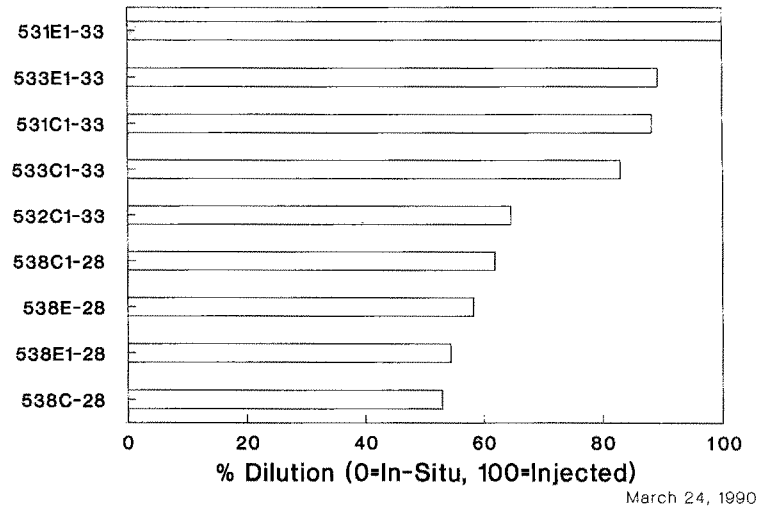

Fig. 22—A normalized dilution of brine produced in the seven-pattern, 5-acre waterflood pilot. Note that Well 531E1-33 produces pure injected water.

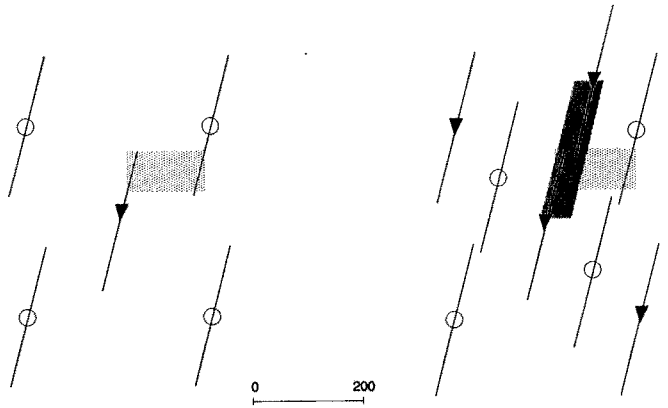

Fig. 23—Producer-injector coupling on 1¼-acre spacing may preclude a future 5-acre development.

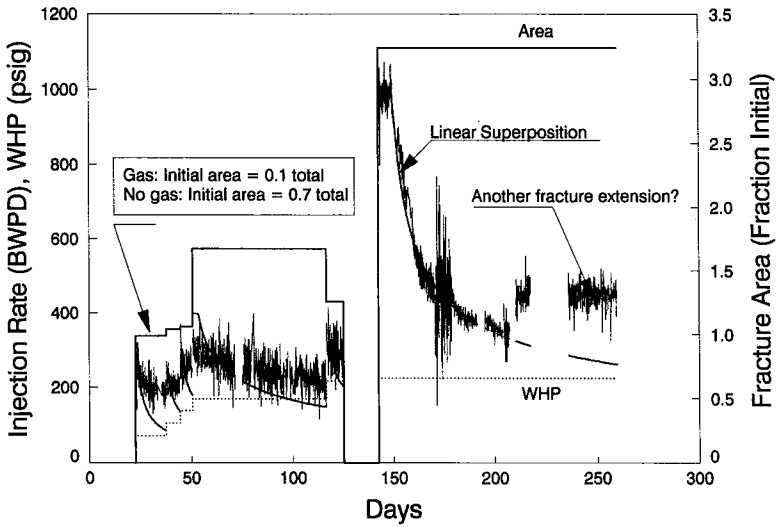

Fig. 24—Injection rate and fracture extensions during four pressure steps in Phase I injector 555E-33. Note that in the worst case the fracture area could be twice the design area.

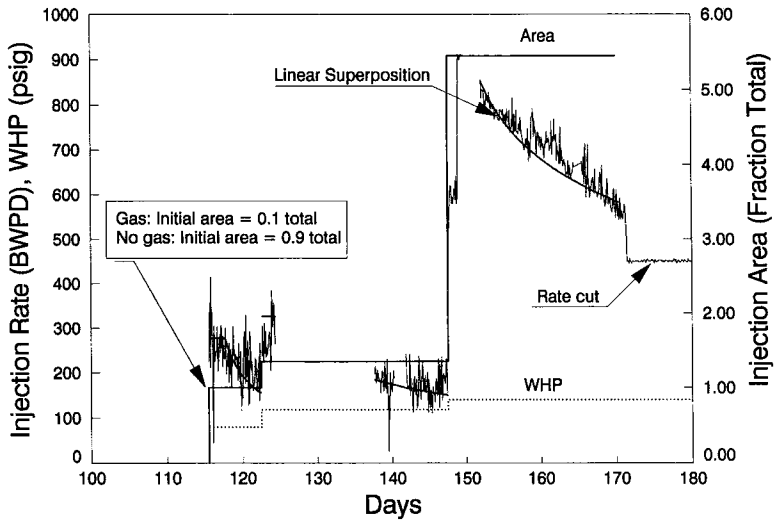

Fig. 25—Injection rate and fracture extensions during two pressure steps in Phase IIIA injector 537E-34. Note that in the worst case the fractures could grow up to five times the design area.

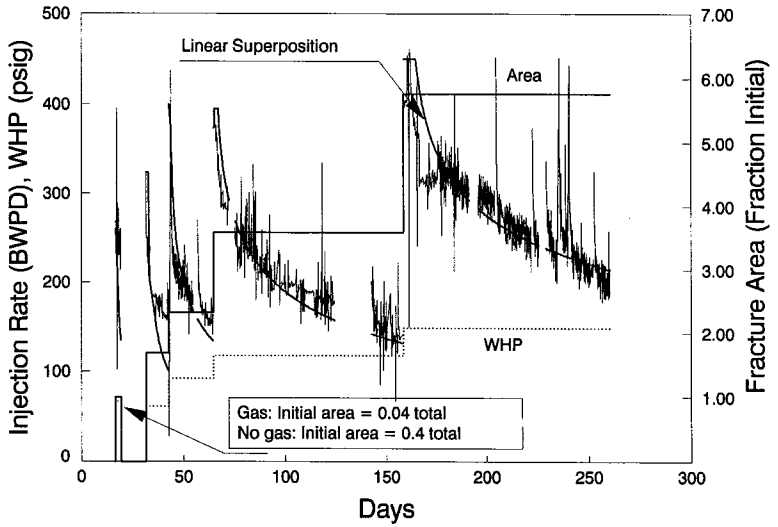

Fig. 26—Injection rate and fracture extensions during four pressure steps in seven-pattern, ⅝-acre waterflood pilot injector 531A1-33. Note that in the worst case the fracture area could be twice the design area.